ORIGINAL ARTICLE

Evaluating the biocompatibility and biological performance of FePt-decorated nano-epoxy nanoparticles in mesenchymal stem cells

Ruey-Hwang Chou[a,b,c], Meng-Yin Yang[d,e,f], Yi-Ping Yang[g], Chun-An Yeh[a], Wei-Yi Lai[g], Tzu-Wei Lin[g], Yuan-Chi Teng[g], Shu-Chen Hsieh[h], Mei-Lang Kung[i], Hsien-Hsu Hsieh[j], Huey-Shan Hung[a,k,*]

[a]Graduate Institute of Biomedical Sciences, China Medical University, Taichung, Taiwan, ROC; [b]Center for Molecular Medicine, China Medical University Hospital, Taichung, Taiwan, ROC; [c]Department of Medical Laboratory and Biotechnology, Asia University, Taichung, Taiwan, ROC; [d]Neurological Institute Head of Department of Neurosurgery Taichung Veterans General Hospital, Taichung, Taiwan, ROC; [e]College of Nursing, Central Taiwan University of Science and Technology, Taichung, Taiwan, ROC; [f]College of Medicine, National chung Hsing University, Taichung, Taiwan, ROC; [g]Department of Medical Research, Taipei Veterans General Hospital, Taipei, Taiwan, ROC; [h]Department of Chemistry, National Sun Yat-Sen University, Kaohsiung, Taiwan, ROC; [i]Department of Medical Education and Research, Kaohsiung Veterans General Hospital, Kaohsiung, Taiwan, ROC; [j]Blood Bank, Taichung Veterans General Hospital, Taichung, Taiwan, ROC; [k]Translational Medicine Research, China Medical University Hospital, Taichung, Taiwan, ROC

Abstract

Background: Nanoparticles have wide potential applications in biolabeling, bioimaging, and cell tracking. Development of dual functional nanoparticles increases the versatility.

Methods: We combined the fluorescent property of nano-epoxy (N-Epo) and the magnetic characteristic of FePt to fabricate the FePt-decorated N-Epo (N-Epo-FePt). The size in diameter of N-Epo-FePt (177.38 ± 39.25 nm) was bigger than N-Epo (2.28 ± 1.01 nm), both could be absorbed into mesenchymal stem cells (MSCs) via clathrin-mediated endocytosis and have multiple fluorescent properties (blue, green, and red).

Results: N-Epo-FePt prevented N-Epo-induced platelet activation, $CD68^+$-macrophage differentiation in blood, and intracellular ROS generation in MSCs. The induction of apoptosis and the inhibitory effects of N-Epo-FePt on cell migration, MMP-9 activity, and secretion of SDF-1α were less than that of N-Epo in MSCs.

Conclusion: N-Epo-FePt was more biocompatible without altering biological performance than N-Epo in MSCs. These results suggest that N-Epo-FePt nanoparticle can be used for fluorescence labeling of MSCs and is potential to apply to bioimaging and cell tracking of MSCs in vivo by magnetic resonance imaging or computed tomography.

Keywords: Biocompatibility; FePt-decorated nano-epoxy; Mesenchymal stem cells; Nano-epoxy; Nanoparticle

1. INTRODUCTION

Epoxy is a popular thermoset resin formed through polymerization reactions. The main molecular structure of epoxy is a high-molecular polymer with aliphatic, aromatic, or alicyclic as the main chain containing two or more oxirane ring groups.[1] Epoxy resin has the characteristics of easy hardening, good adhesion and mechanical properties, low volume shrinkage, insulation properties, and resistance to acid and alkali chemicals.[2] It has been widely used for industrial applications including coatings,[3,4] electronic devices,[5] marine systems,[6] and aerospace parts.[7] Epoxy nanocomposites have also been applied in biomedical applications. For instance, polymer particles with grafted epoxy polymer chains provided a three-dimensional microenvironment to promote the growth and differentiation of hematopoietic stem cells.[8] Covalent conjugation of an epoxy-based negative photoresist, SU-8, with fibronectin and collagen type I matrix proteins enhanced adhesion and proliferation of mesenchymal stem cells (MSCs).[9] Modification of magnetite-polymer Fe_3O_4-poly-ε-caprolactone with amino and epoxy groups allowing easy covalent attachment of specific antibodies for selective isolation of subpopulations of human adipose-derived stem cells.[10] In addition, epoxy containing nanodots exhibited a broad band, and multifluorescence properties, which were beneficial to label cells for biosensing.[11]

Iron platinum (FePt) nanoparticles (NPs) have been widely studied in biomedicine. They have characteristics of high Curie temperature, saturation magnetic moment, good magnetocrystalline anisotropy, high coercivity, and high magnetic energy.[12] In addition, due to the good biocompatibility, superparamagnetic, and high X-ray absorption properties, FePt nanoparticles have applied as a dual modality contrast agent for magnetic resonance imaging (MRI) and computed tomography (CT).[13] Water-soluble

*Address correspondence. Dr. Huey-Shan Hung, Graduate Institute of Biomedical Science, China Medical University, 6, Hsueh-Shih Road. Taichung 404, Taiwan, ROC. E-mail address: hunghs@mail.cmu.edu.tw (H.-S. Hung).

Author contributions: Dr. Ruey-Hwang Chou and Dr. Meng-Yin Yang contributed equally to this work.

Conflicts of interest: The authors declare that they have no conflicts of interest related to the subject matter or materials discussed in this article.

Journal of Chinese Medical Association. (2021) 84: 1109-1119.

Received August 16, 2021; accepted September 16, 2021.

doi: 10.1097/JCMA.0000000000000627.

L-cysteine coated FePt (FePt-Cys) nanoparticles were developed as MRI/CT imaging contrast agent for the diagnosis of malignant gliomas.[14] Encapsulation of FePt nanoparticles with PEGylated phospholipids to generate stealth immunomicelles was reported to detect human prostate cancer cells by MRI and fluorescence imaging.[15] Superparamagnetic FePt nanoparticles (SIPPs) were used as vectors for encapsulated paclitaxel (PTX) to produce multifunctional SIPP-PTX micelles combined with an antibody against a prostate-specific membrane antigen for detection by MRI and specific targeting therapy in the xenograft mice model of human prostate cancer.[16]

Mesenchymal stem cells can self-renew and differentiate into specific cell lineages, such as bone, adipocytes, and neuron.[17] Moreover, MSCs have broad anti-inflammatory and immunemodulatory properties, in which they selectively migrate toward the site of injury, namely "homing" process.[18] Due to the aforementioned characteristics, MSCs have been considerably inspected as potential biomedical applications for cell-based therapies of inflammatory, immune-mediated, and degenerative diseases and cancers. To detect and track MSCs, several labeling methods of MSC were developed. Expression a fluorescent protein, green fluorescent protein, by lentivirus-delivery into human umbilical cord-derived MSCs has been used for long-term *in vitro* labeling, and may serve as a fluorescent tracker following transplantation *in vivo*.[19] Thulium ion (Tm^{3+})-based nanoparticles were designed for deep tissue penetration as large as 2 mm of fluorescence bioimaging excited with near-infrared near-infrared.[20] In addition to fluorescence labeling, Gadolinium ion (Gd^{3+})-containing carbon nanotube was evolved as MRI contrast agent for stem cells labeling.[21]

In the current study, we aimed to innovate dual functional nanoparticles combined the fluorescent property of nano-epoxy (N-Epo) and the magnetic characteristic of FePt to fabricate the FePt-decorated N-Epo (N-Epo-FePt) nanoparticles for biomedical applications and determine their physical characteristics, biocompatibility, biological effects in MSCs.

2. METHODS

2.1. Preparation of Nano-Epoxy and Nano-Epo-FePt

The Nano-Epoxy and Nano-Epoxy-FePt nanoparticles were kindly provided by Professor Shu-Chen Hsieh. In brief, 3-Glycidoxypropyl trimethoxysilane-containing self-assembled SiOx nanodots (GPS-SANDs) were synthesized by the one-step heat procedure as followings, 3 mL GPS (Sigma) was stirred in a glass vial at 1000 rpm at 350°C for 90 minutes under an ambient air atmosphere. Afterward, the sample was slowly cooled to room temperature with continuously gently stirring to generate GPS-SANDs as Nano-Epoxy.[11]

2.2. Characterization of Physical Properties

2.2.1. Transmission Electron Microscopy

The solution of N-Epo or N-Epo-FePt nanoparticles (0.5 μL) were dropped onto a carbon grid with 200 copper mesh (No. 01801, Ted Pella Inc.) for drying. The dried samples were applied to collect transmission electron microscopy (TEM) images under a JEOL JEM-2100 electron microscope with the conditions of 200 kV at 2×10^{-5} Pa vacuum as previous study.[11]

2.2.2. Photoluminescence Intensity

The PL spectra were scanned with the excitation wavelengths from 340 nm to 540 nm at 20 nm intervals by the F-7000 fluorescence spectrometer (Hitachi). The emission spectra were collected with the wavelengths from 200 nm to 800 nm, followed by measuring the (PL) intensity.[11]

2.2.3. Atomic Force Microscopy

The size of N-Epo or N-Epo-FePt nanoparticles were determined by an atomic force microscopy (AFM) (MFP-3D, Asylum Research). Ten microliters of nanoparticles in toluene solution (nanoparticles: toluene = 1:200, V/V) were dropped and sprayed onto a silicon wafer substrate. The images (512 × 512 pixels) were scanned at 1.0 Hz scan rate by a silicon cantilever (Olympus, AC240TS) with nominal spring constant of 2 N/m by an AFM with tapping mode under ambient conditions.[11]

2.2.4. Dynamic Light Scattering

The aqueous solution of N-Epo or N-Epo-FePt nanoparticles (0.2 mg/mL) was filtrated through a 0.45 μm filter (Millipore). The size distribution of these nanoparticles was determined with dynamic light scattering (DLS) by using Zetasizer Nano ZS90 (Malvern Panalytical, United Kingdom). The data were acquired with a He–Ne laser (633 nm) and 90° collecting optics at 25°C and analyzed by Zetasizer software (Malvern Panalytical).

2.3. Immunofluorescence Staining for Uptake Assay and Inhibitor Assay

For uptake assay, cells were seeded on a 15 mm coverslip at a density of 2×10^4 cells/well in a 24-well plate, and then treated with N-Epoxy or N-Epoxy-FePt nanoparticles for 2 or 24 hours. For inhibitor assay, the neutralization effect of chlorpromazine (Sigma), methyl-β-cyclodextrin (Sigma), cytochalasin D (CCD) (Sigma), and Bafilomycin (Sigma) in response to MSCs after uptake of N-Epoxy and N-Epoxy-FePt nanoparticles were examined. MSCs were seeded on a 15-mm coverslip at a density of 2×10^5 cells/well in a 24-well plate, and then pretreated with 2 μM chlorpromazine (CPZ), 2.5 mM methyl-β-cyclodextrin (MβCD), 5 μM CCD, or 100 nM Bafilomycin (Bafa) for 1 hour at 37°C. Subsequently, the medium was replaced with fresh culture medium and cells were incubated for another 2 or 24 hours. After treatment, cells were applied to immunofluorescence staining as below, treated cells were washed with Phosphate-Buffered Saline (PBS), followed by fixation with 4% paraformaldehyde (Sigma) for 15 minutes, and permeabilization with 0.5% (v/v) Triton X-100 (Sigma) in PBS for 10 minutes. The fixed cells were blocked with 1% (w/v) bovine serum albumin at room temperature for 30 minutes, and then stained with rhodamine phalloidin (1:1000, Sigma) for 30 minutes. Finally, the coverslips were mounted onto slides after extensively washing, and conducted to obtain images under a fluorescence microscope (Eclipse 80i, Nikon, Japan).[22]

2.4. Biocompatibility Assays

2.4.1. 3-(4,5-dimethylthiazol-2-yl)-2,5-diphenyltetrazolium bromide Assay for Cell Viability

3-(4,5-dimethylthiazol-2-yl)-2,5-diphenyltetrazolium bromide (MTT) assay was performed to measure cell viability. MSCs were seeded at a density 1×10^4 per well of into a 96-well dish on a day before experiments. Cells were then treated with different concentrations of N-Epoxy or N-Epoxy-FePt nanoparticles for 24, 48, and 72 hours. After treatment, the medium was replaced with fresh medium containing 0.5 mg/mL of MTT and incubated at 37°C for another 2 hours. After discarding the medium, the formazan crystals within cells were dissolved with dimethyl sulfoxide (DMSO) and the absorbance was measured at 570 nm by a microplate reader (SpectraMax M2e, Molecular Devices, USA). The cell viability was calculated by the relative fold change of OD570 in the experimental group comparing to that in the control group.[23]

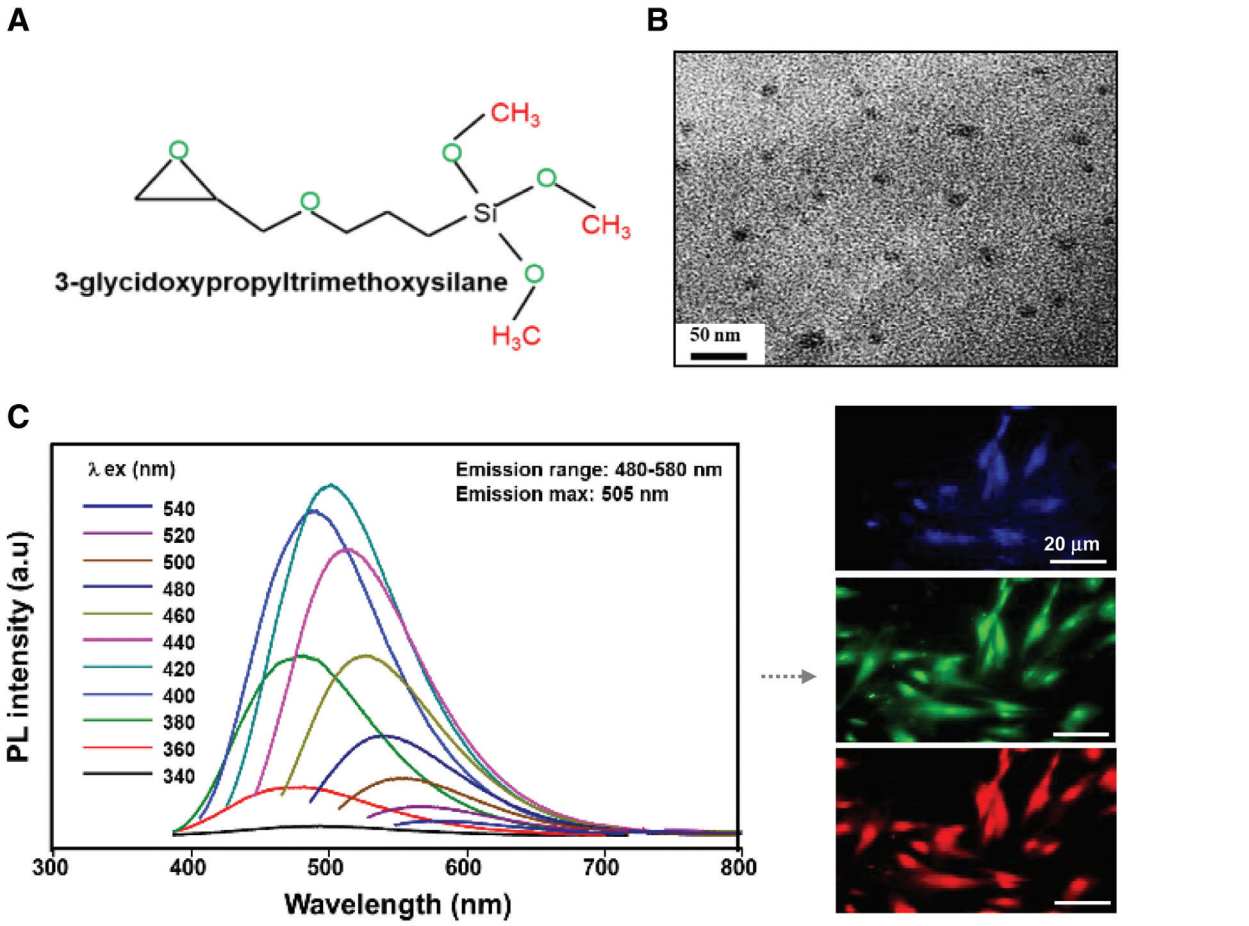

Fig. 1 Characterization of N-Epo. A, Chemical structure of GPTMS, (B) the image of N-Epo under a TEM, (C) photoluminescence spectrum of N-Epo (left); the schematic diagram in the N-Epo treated MSCs under blue, green, and red emission wavelengths (right). N-Epo = nano-epoxy; GPTMS

2.4.2. Platelet Activation Assay

Platelet activation assay was determined as previously described.[23] Platelet-rich plasma were obtained from the Taichung Veterans General Hospital, Taiwan. In brief, the indicated concentrations of N-Epoxy or N-Epoxy-FePt nanoparticles and 0.5 mL of platelet-rich plasma (2×10^6 platelets/mL) were added in a 24-well plate and incubated at 37°C for 1 hours. Subsequently, the number of adherent platelets was calculated by a cell counter (Assistant, Germany).

Inflammatory index was performed as previously described.[23] Monocytes were isolated from whole blood of healthy donors (IRB approval number CE12164) by density gradient centrifugation in Percoll solution (Sigma). The purified monocytes were seeded at a density of 1×10^5 cells/mL onto the N-Epoxy or N-Epoxy-FePt nanoparticles coated 24-well culture plate and incubated at 37°C for 96 hours. Afterward, the cells were collected and the numbers of monocytes and macrophages were counted based on the morphology under an inverted phase contrast microscope. The inflammatory index was calculated by the ratio of macrophages to monocytes. The expression of CD68 on macrophages after incubation with N-Epoxy or N-Epoxy-FePt nanoparticles for 96 hours was examined by immunofluorescence staining with primary antibody against CD68 and FITC-conjugated secondary antibody. Cell nuclei were counterstained by DAPI (4′, 6-diamidino-2-phenylindole) staining.

2.4.3. ROS Measurement

Intracellular reactive oxygen species (ROS) were determined by the cell-permeable fluorogenic probe 2′,7′-dichlorofluorescin diacetate (DCFH-dA) (Sigma) as previously described.[23] MSCs were seeded at a density of 2×10^5/well into a 96-well dish on a day before experiments. Cells were treated with different concentrations of N-Epoxy or N-Epoxy-FePt nanoparticles and incubated at 37°C for 48 hours. Afterward, cells were collected, washed with PBS, and incubated with 10 μM of DCFH-dA at 37°C for 30 minutes. The intracellular ROS was determined according to the fluorescence intensity from excitation/emission wavelength of 480 nm/530 nm at 30 minutes intervals for 4 hours by a fluorescence activated cell sorter (FACS) Calibur flow cytometer (Becton Dickinson, USA). The fluorescent cells were further quantified by the CellQuest software (Becton Dickinson, USA).

2.5. Cell Cycle Analysis and Cell Toxicity Test

Distribution of the cells in each phase of the cell cycle was determined by a flow cytometer. In brief, 2×10^5 cells were collected, fixed with 80% ethanol in PBS, and then stained with 0.2 mL of propidium iodide (PI) solution containing 0.05 mg/mL PI, 1 mg/mL RNase A, 1 mM EDTA, and 0.01% Triton X-100 in PBS for 1 hour, followed by a FACS Caliber flow cytometer (Becton Dickinson) analysis. The distributions of cells in G1, S, and G2/M phases of cell cycle were analyzed by FACS software, and cells with subdiploid DNA content were considered as apoptotic cells in sub-G1 phase.[22]

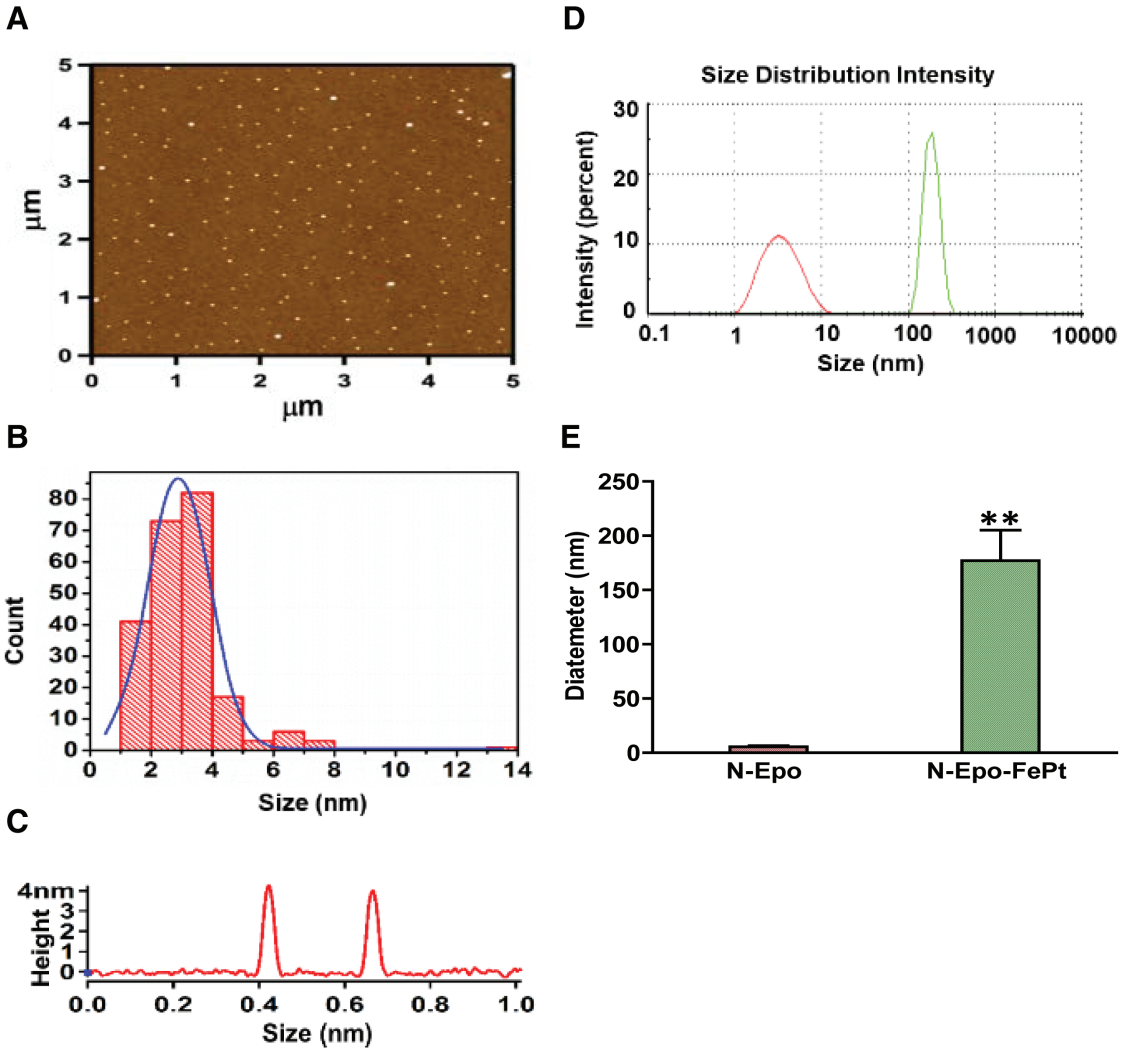

Fig. 2 Characterization of nano-epoxy by AFM and DLS. (A) Image of surface topography of N-Epo, (B) the distribution of the particle size of N-Epo, (C) the height of Nano-epoxy, (D) the distribution of the particle size of N-Epo (red) and N-Epo-FePt (green) measured by DLS, (E) the quantitative result of N-Epo (red bar) and N-Epo-FePt (green bar) particle size. $^{**}p < 0.01$ comparing to that of N-Epo.

The cell toxicity test was performed as annexin V/PI staining as previously described.[22] MSCs were treated with or without N-Epoxy or N-Epoxy-FePt nanoparticles. Afterward, cells were stained with FITC-conjugated antiannexin V antibody and PI solution, and the images were observed under a fluorescence microscope. Annexin V-positive cells were considered as apoptotic cell death. For the cytometric analysis of apoptotic cell death, treated cells were collected, stained with FITC-conjugated anti-Annexin V antibody and PI solution, and then subjected to a flow cytometric analysis. Accordingly, cells were considered as live cells with Annexin V negative/PI negative, early apoptotic cells with Annexin V negative/PI positive, late apoptotic cells with Annexin V positive/PI positive, and necrotic cells with Annexin V negative/PI positive.

2.6. Assays for Biological Functions

2.6.1. Cell Migration Assay

Cell migration assay was performed by wound healing with Oris tricoated plate (Platypus technologies, USA).[23] A cell seeding stopper was inserted in the center on top of Oris plate, and cells were then seeded onto the plate at a density of 8×10^3/well and cultured for 24 hours to full confluence. Initially, the stopper was removed from the experimental well, but kept one well with stopper as the premigration reference. Subsequently, cells were treated with or without N-Epoxy or N-Epoxy-FePt nanoparticles, and incubated at 37°C for different time intervals (0, 24, 48 hours). After treatment, cells were labeled with 2 mM Calcein-AM and the image was obtained at each time interval under a fluorescence microscope (Zeiss Axio Imager A1, USA). The distance of cell migration inside the boundary was quantified by Image Pro Plus 5.0 software.

2.6.2. Detection of Secreted SAF-1 Protein

The secreted SDF-1 was determined with human CXCL12/SDF-1 DuoSet ELISA Development System kit (R&D system). MSCs were treated with or without N-Epoxy or N-Epoxy-FePt nanoparticles for 48 hours. The conditioned media were collected for detection of secreted SAF-1 protein according to the instruction of the kit. The OD value were measured at 450 nm by using an ELISA reader.

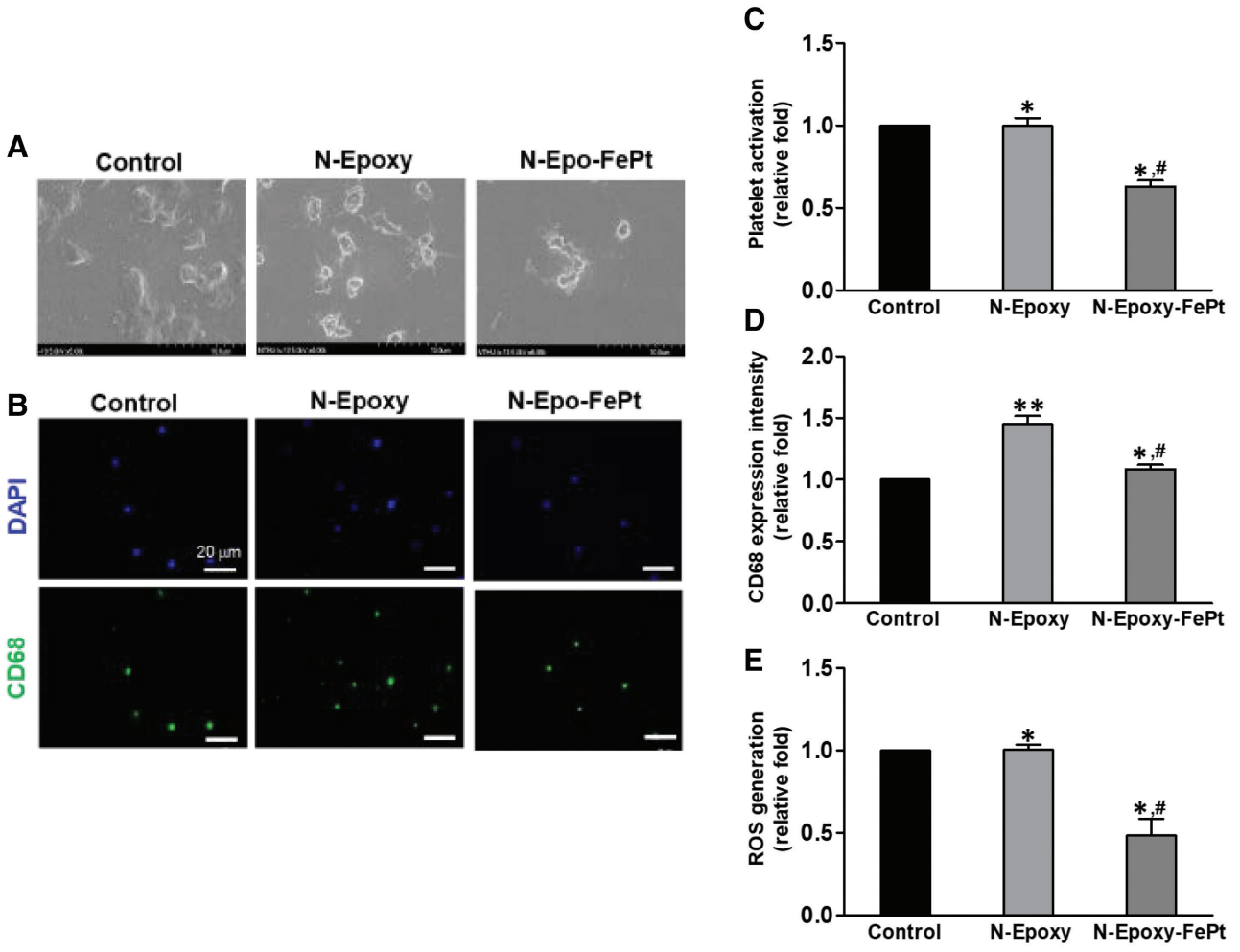

Fig. 3 Validation of biocompatibility of nano-epoxy. (A) The representative image of adherent platelets on uncoated (control), N-Epo-coated, and N-Epo-FePt-coated well. (B) The relative platelet activation was determined by relative fold of adherent platelets. (C) Approximate 10^5 monocytes were cultured in the medium with or without N-Epo and N-Epo-FePt for 96h. The expression of a macrophage marker, CD68, was determined by immuno-fluorescent staining (green color). The cell nucleus was counterstained with DAPI (blue color). (D) The relative CD68 expression was quantified. (E) MSCs were treated with 15000-fold diluted N-Epo or N-Epo-FePt for 48 hours. Subsequently, the amount of intracellular ROS was measured as oxidization of DCFDA to fluorescent DCF by a flow cytometer. The relative ROS generation was shown. *p<0.05, ***p<0.001; #p<0.05, ##p<0.01 in comparison with untreated cells (control) and N-Epo treated cells, respectively.

2.6.3. Gelatin Zymography

Approximately, 2 ×10^5 cells were seeded into a 10-cm culture dish on a day before experiments. After treatment for 48 hours, the conditioned medium was collected and applied to gelatin zymography as previously described.[23] The conditioned media were separated by SDS-PAGE with 2% gelatin. After separation, the gelatin gel was incubated in the Zymogram renaturing buffer containing 40 mM Tris-HCl, pH8.5, 0.2 M NaCl, 10 mM $CaCl_2$, and 2.5% Triton X-100 with gentle agitation at room temperature for 30 minutes by two times. The gelatin gel was equilibrated in the 1 × Zymogram developing buffer containing 40 mM Tris-HCl, pH 8.5, 0.2 M NaCl, 10 mM $CaCl_2$, and 0.01% NaN_3) with gentle agitation at room temperature for another 30 minutes, and then immersed with fresh developing buffer and incubated at 37°C overnight. Subsequently, the gel was stained with 0.2% Coomassie brilliant blue R-250 in 10% acetic acid and 50% methanol and then washed in destaining solution (10% acetic acid, 20% methanol). The clear bands represented the gelatin digested areas by activated MMPs. The stained gelatin gel was scanned by a densitometer and the clean areas were quantified by Image Pro Plus 5.0 software (Media Cybernetics). The quantified data were normalized by total proteins in the conditioned media.

2.7. Statistical Analysis

Data were showed as mean ± SD. The differences between mean values of experimental and control groups were determined with one-way ANOVA and Scheffe test by SPSS software (version 17.0). Probability value (p) < 0.05 was consider as statistical significance between groups.

3. RESULTS

3.1. Characterization of Nano-epoxy and Nano-epoxy-FePt

Nano-epoxy (N-Epo) was fabricated from an epoxy resin, 3-glycidoxypropyltrimethoxysilane (GPTMS) (Fig. 1A). The results from TEM showed the evenly distributed image less than 50 nm in diameter of N-Epo (Fig. 1B).

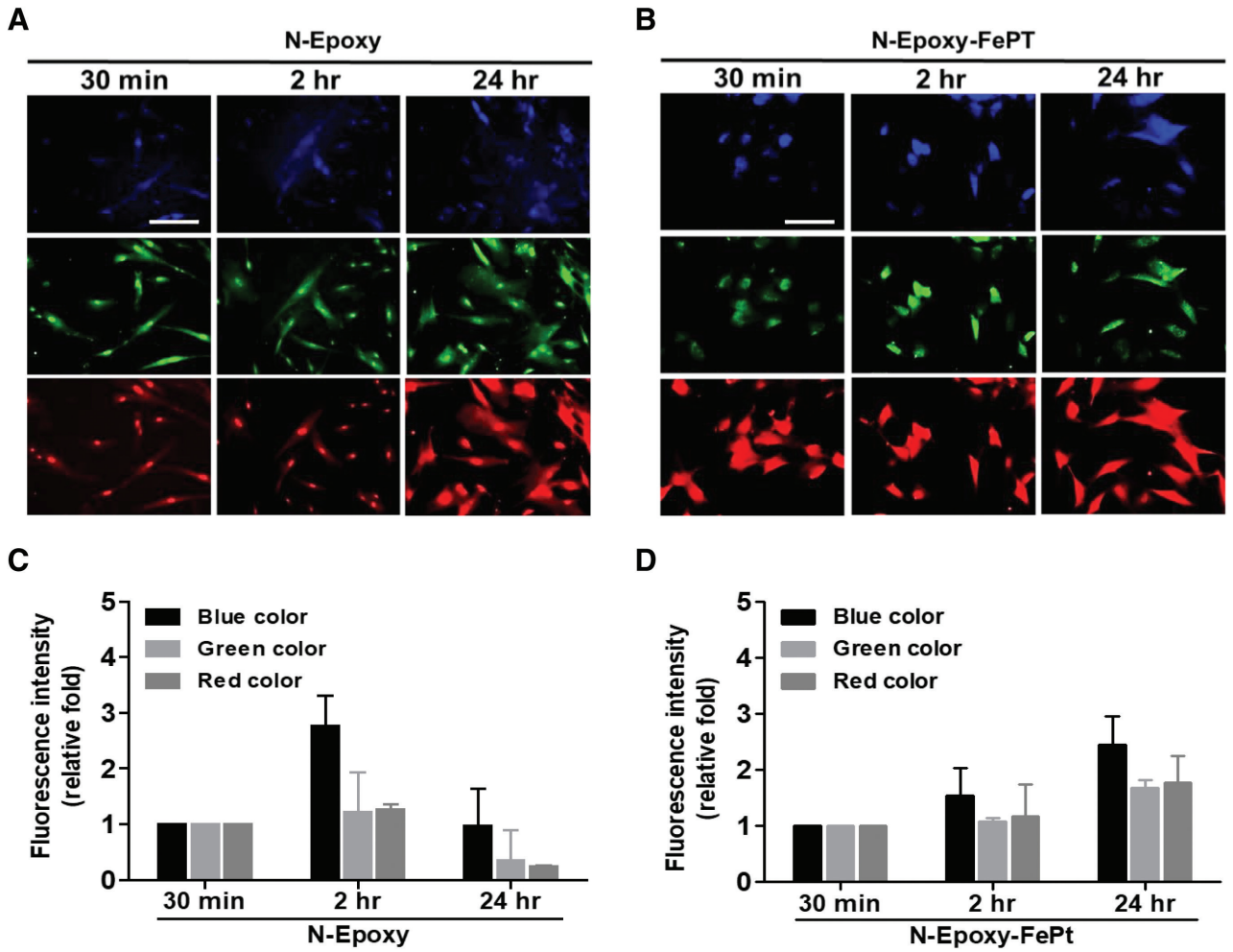

Fig. 4 The cellular uptake of N-Epo and N-Epo-FePt in MSCs. MSCs were treated with 15000× diluted N-Epo (A and C) and N-Epo-FePt (B and D) for 30 min, 2 h, or 24 h. (A and B) The fluorescent images were captured under a fluorescence microscope with different emission wavelengths (blue, green, and red colors). (C and D) Fluorescence activated cell sorter (FACS) assay was also applied to observe the uptake efficiency was also quantified based on fluorescent intensity by immunofluorescence by flow cytometry. The plots represented the relative fold change of fluorescence intensity by mean ± SD.

The photoluminescence (PL) spectrum of N-Epo revealed that the emission wavelengths of N-Epo were ranged from 480 nm to 580 nm and peaked at 505 nm, indicating the multiple fluorescent properties of N-Epo (Fig. 1C, left panel), and the schematic diagram was shown in the N-Epo treated MSCs under blue, green, and red emission wavelengths (Fig. 1C, right panel). The physical properties of nano-epoxy were further characterized by AFM and DLS. The image from AFM showed the surface topography of N-Epo (Fig. 2A) with 3.1 ±1.4 nm in diameter (Fig. 2B) and 3.9 nm in height (Fig. 2C). The results from DLS demonstrated that the size distribution of N-Epo-FePt was extremely larger than N-Epo (Fig. 2D) with 177.38 ± 39.25 nm and 2.28 ± 1.01 nm in diameter, respectively (Fig. 2E).

3.2. Validation of Biocompatibility of Nano-epoxy

To determine the biocompatibility of N-Epo and N-Epo-FePt, the effects on platelet activation, macrophage activation, and cytotoxicity were examined. The well coated with N-Epo-FePt significantly reduced platelet activation as determined by the numbers of adherent platelets; however, N-Epo-coated well did not (Fig. 3A, C). In terms of macrophage activation, more N-Epo-treated monocyte differentiated to CD68-positive macrophage than N-Epo-FePt-treated one (Fig. 3B, D), suggesting that FePt-decorated N-Epo could prevent N-Epo-induced inflammation. Moreover, the intracellular ROS were markedly less in N-Epo-FePt-treated MSCs than that in N-Epo-treated one (Fig. 3E). The results from MTT assay showed that 2500×-, 5000×-, and 10 000×-diluted N-Epo and N-Epo-FePt were toxic to MSCs after 24, 48, or 72 hours treatment, while the cytotoxicity was limited or nontoxic at 15 000×-dilution (Supplementary Fig. 1, http://links.lww.com/JCMA/A111). Taken together, based on the lower platelet activation, macrophage differentiation, and less intracellular ROS generation by N-Epo-FePt, FePt-decorated N-Epo was more biocompatible than N-Epo.

3.3. The Uptake of N-Epo and N-Epo-FePt Into MSCs Is Mainly Through Clathrin-mediated Endocytosis

To determine the uptake of nano-epoxy into MSCs, the fluorescent images were obtained after treatment of N-Epo (Fig. 4A) or N-Epo-FePt (Fig. 4B) for different time intervals. The results showed that both N-Epo and N-Epo-FePt could be absorbed into MSCs after 30 minutes and their multiple fluorescent

properties were also observed at blue, green, and red wavelengths. The quantitative results indicated that the fluorescence peaked at 2 hours and sustained for 24 hours in N-Epo treated MSCs (Fig. 4C), while the fluorescence increased with time from 30 minutes to 24 hours in N-Epo-FePt treated MSCs (Fig. 4D). In short, both N-Epo and N-Epo-FePt could be absorbed into MSCs after 30 minutes and were stable at least for 24 hours within cells.

To further clarify the possible pathways of the uptake of nano-epoxy into MSCs, the selective inhibitors, CPZ and bafilomycin A (Baf) against clathrin-mediated endocytosis (CME), CCD against phagocytosis-macropinocytosis, or beta-methyl-cyclodextrin (β-MCD) against caveolae-dependent endocytosis, were tested. Pretreating MSCs with CPZ or Baf significantly disrupted the uptake of N-Epo-FePt after treatment for 2 hours (Fig. 5A, C) and 24 hours (Fig. 5B, D). However, pretreatment of β-MCD or CCD did not affect the uptake of N-Epo-FePt into MSCs. Similar phenomena were also observed in the uptake of N-Epo into MSCs (Supplementary Figure 2, http://links.lww.com/JCMA/A111). Taken together, the uptake of N-Epo-FePt and N-Epo was mainly through clathrin-mediated endocytosis in MSCs.

3.4. The Effects of N-Epo and N-Epo-FePt on Cytotoxicity and Cell Cycle Progression in MSCs

To distinguish the cell death caused by nano-epoxy in MSCs, annexin V/PI staining was performed. The results showed that most of MSCs were viable after 48 hours treatment (annexin V–, PI–). Nano-epoxy induced apoptotic cell death (annexin V+, PI±), but not necrosis (annexin V–, PI+), whereas the apoptosis was

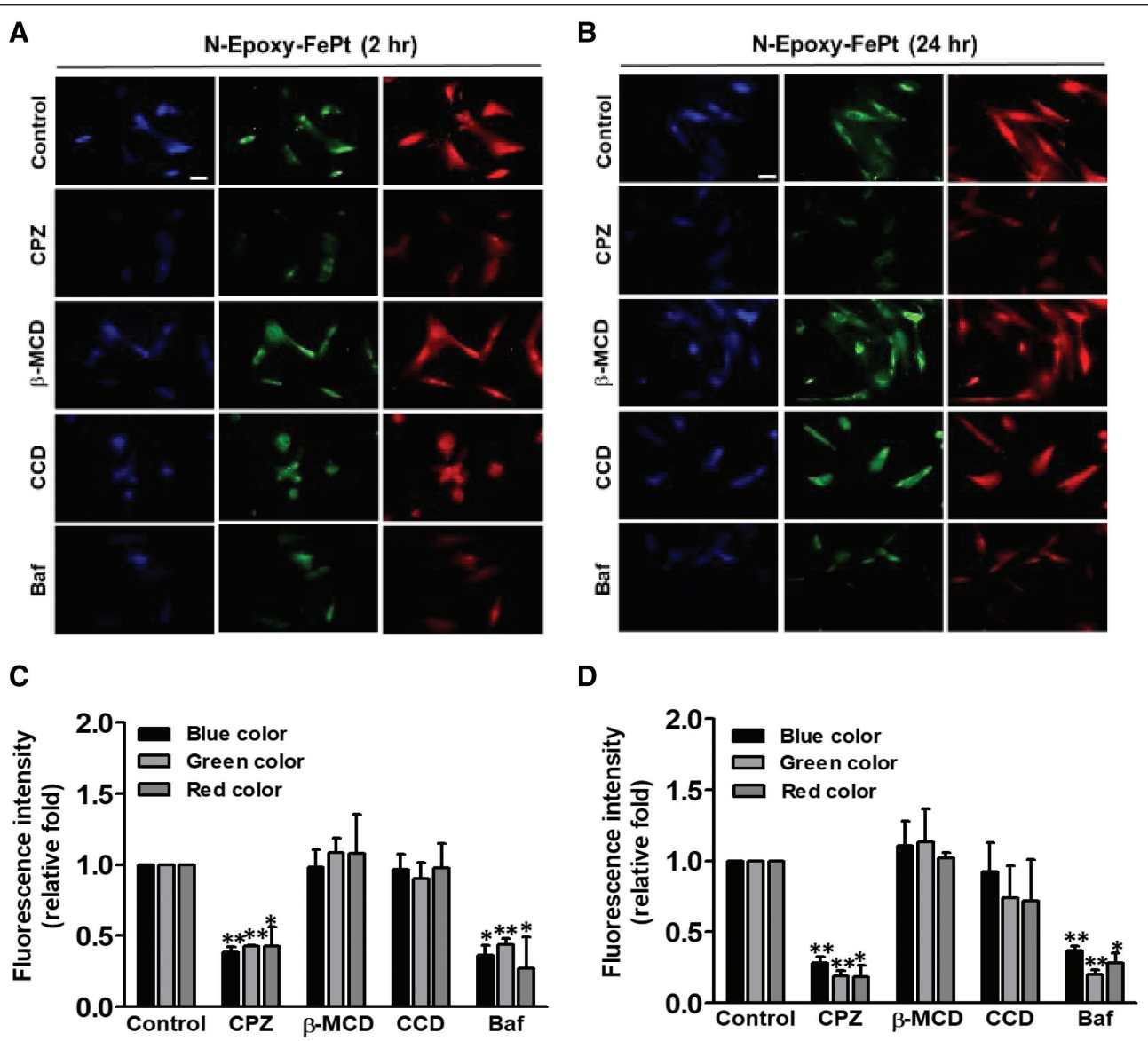

Fig. 5 The cellular uptake of N-Epo-FePt is mainly through clathrin-mediated endocytosis. MSCs were pretreated with the selective inhibitors of clathrin-mediated endocytosis (CME), chlorpromazine (CPZ), and bafilomycin A (Baf), or inhibitors of phagocytosis-macropinocytosis and caveolae-dependent endocytosis, cytochalasin-D (CCD), and beta-methyl-cyclodextrin (β-MCD), respectively, for 1 h, and then treated with N-Epo-FePt for another 2 h (A) or 24 h (B). (A and B) The fluorescent images in each time interval were captured under a fluorescence microscope with different emission wavelengths (blue, green, and red colors). (C and D) Fluorescence intensity influenced by various inhibitors was also analyzed by flow cytometery. *$p < 0.05$, **$p < 0.01$. The bar plots represented the relative fold change of fluorescence intensity comparing to that from control cells by mean ± SD (*$p < 0.05$; **$p < 0.01$).

less in N-Epo-FePt-treated MSCs than that in N-Epo-treated one (Fig. 6A, C). In addition, the cells at sub-G1 phase were also less in N-Epo-FePt-treated MSCs comparing to that in N-Epo-treated one without alternation of cell cycle progression at G0/G1, S, and G2/M phases (Fig. 6D). To sum up, N-Epo-FePt and N-Epo were biocompatible and did not alter cell cycle progression in MSCs.

3.5. The Effects of N-Epo and N-Epo-FePt on the Movement of MSCs

The migration of MSCs is important for homing. Therefore, the effects of nano-epoxy on the movement of MSCs were examined. The results from Oris cell migration assay demonstrated that N-Epo-FePt did not inhibit the migratory ability of MSCs, but N-Epo suppressed the boundary moving distance of MSCs comparing to the control cells (Fig. 7A, B). The secreted MMP-9 activity was significantly reduced in the conditioned medium from N-Epo-treated MSCs than that from N-Epo-FePt treated one (Fig. 7C). In addition, the SDF-1α/CXCR4 signaling has been reported to be involved in cell migration. Thus, the secreted SDF-1α was determined by ELISA. The secretion of SDF-1α was lower in the conditioned medium from N-Epo-treated MSCs than that from N-Epo-FePt treated one (Fig. 7D). These results revealed that the inhibitory effects

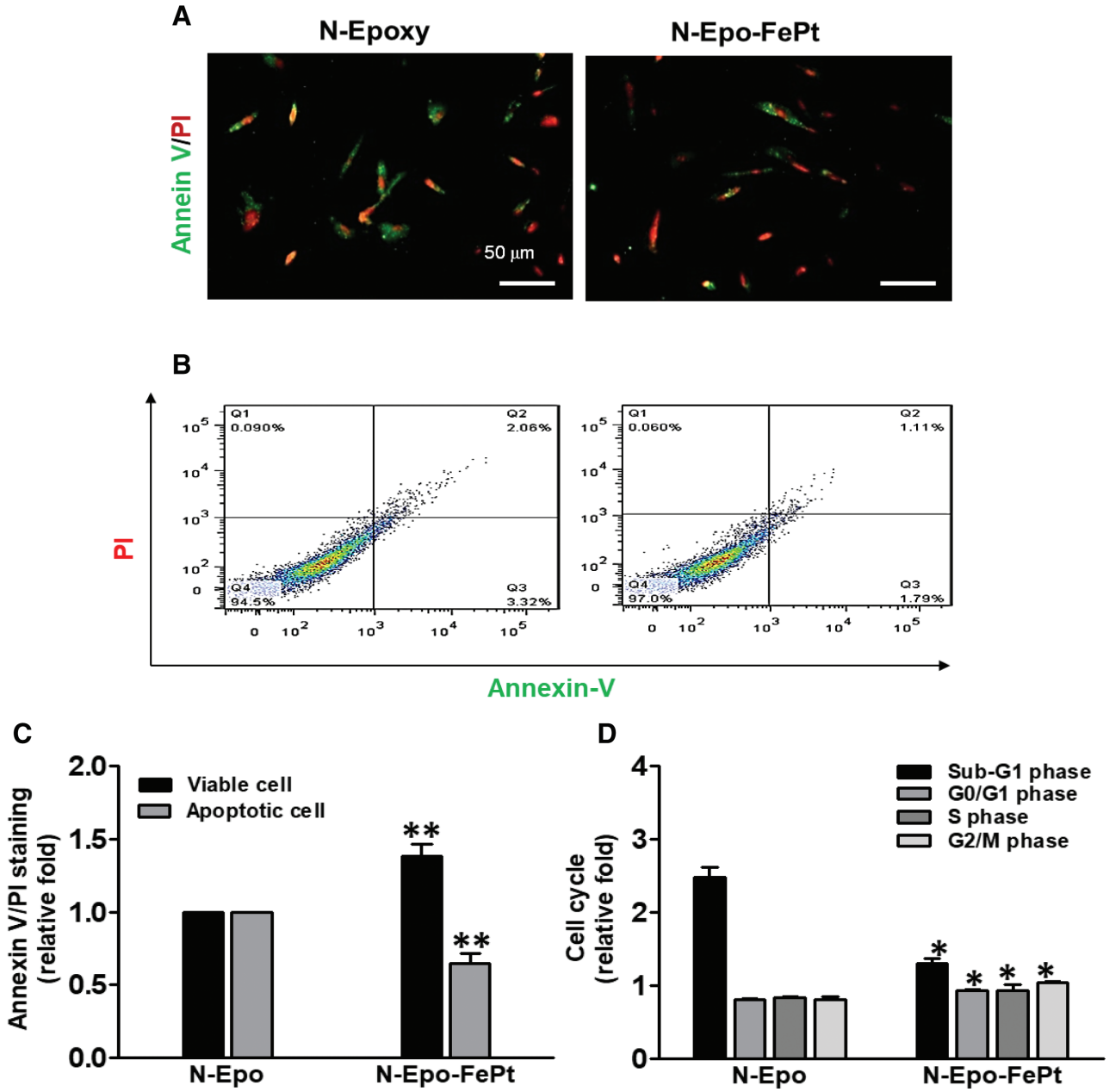

Fig. 6 The effects of N-Epo and N-Epo-FePt on apoptotic cell death and cell cycle progression. MSCs were treated with N-Epo or N-Epo-FePt for 48 h. (A) the representative fluorescent images of cells stained with annexin V and PI. (B) Cells were stained with a FITC-conjugated antiannexin V antibody and PI, followed by a flow cytometric analysis. (C) Cell line was subjected MSCs for 48 h, then double stained by Annexin V (green) –PI (red) for fluorescence microscopy and flowcytometry investigation. Epoxy (alone) could induce more apoptotic (Annexin V^+) and dead (PI^+) cells. $^{**}p < 0.01$. (D) The results evaluated that the amount of apoptotic cells was remarkably increased in especially in Epoxy (alone). Cell cycle influenced by various materials was also analyzed by flow cytometery. Further, cell population of G0/G1 phase was observed more than G2/M, S, and Sub-G1 phase after N-Epo treatment. $^{*}p < 0.05$.

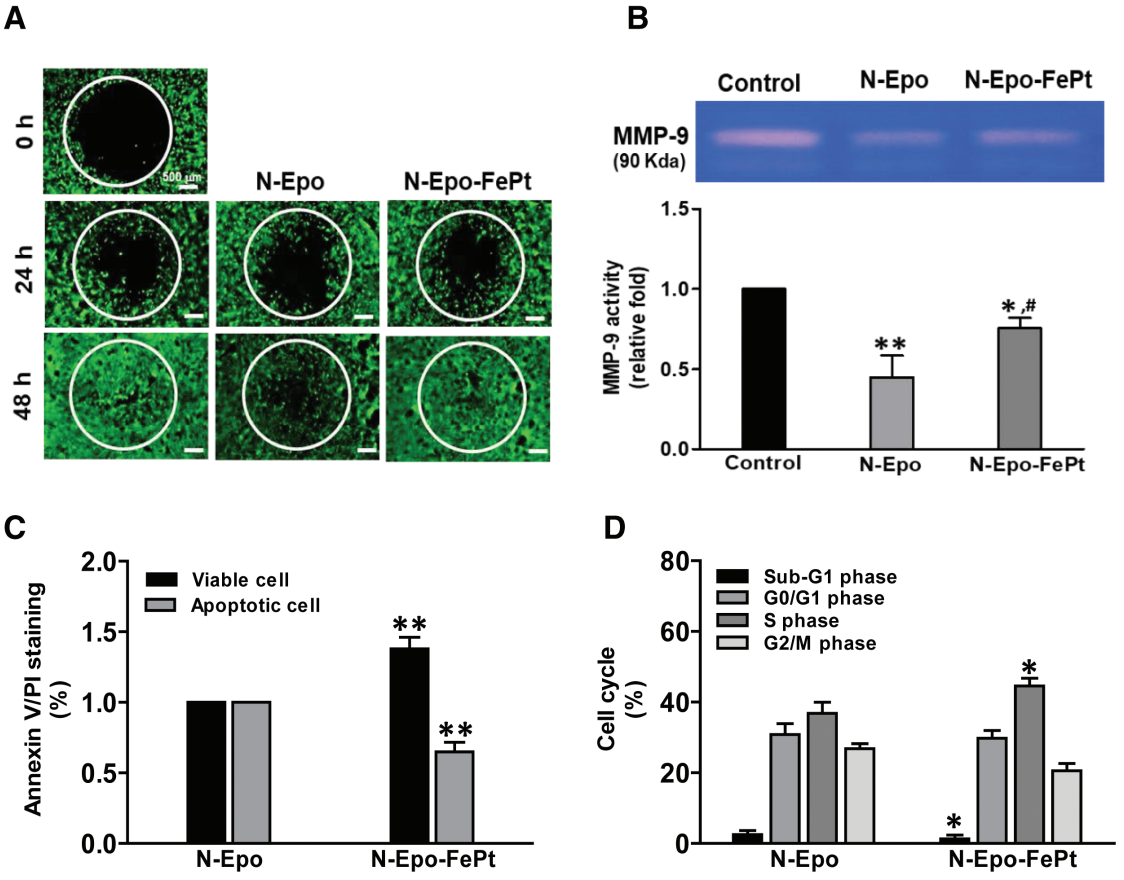

Fig. 7 (A) The effects of N-Ep treatment was determined by Oris cell migration assay. (B) The boundary moving distance of MSCo and N-Epo-FePt on the properties of migration, MMP-9 activity, and SDF-1 α secretion of MSCs. MSCs were treated with or without N-Epo and N-Epo-FePt for 24 and 48 h. (A) The migratory ability of MSCs in eachs in each treatment was quantified. (C and D) The conditioned medium in each treatment was collected. Subsequently, (C) the MMP-9 activity was measured by gelatin zymography. (D) The amount of secreted SDF-1 α protein was examined by ELISA. *p<0.05, **p<0.01; #p<0.05, ##p<0.01 in comparison with untreated cells (control) and N-Epo treated cells, respectively.

of N-Epo-FePt on cell migration, MMP-9 activity, and secretion of SDF-1α were less than that of N-Epo in MSCs.

The summary of the major findings of MSCs by N-Epoxy and N-Epoxy-FePt as illustrated in the Fig. 8.

4. DISCUSSION

Nanoparticles are potential to be used in wide areas including biomedical applications, such as labeling and tracking cells, and delivery of drugs, proteins, DNA, or antibodies. Therefore, biocompatibility and biological performance are important issues to evaluate biosafety and functions of nanoparticles in different cell types. Cytotoxicity, genotoxicity, and immune responses are the general approaches to assess biosafety. For instance, Cytotoxicity is judged by cell viability according to mitochondrial dehydrogenases activity and cell membrane integrity by tetrazolium-based assay (MTT, MTS, or WST-1 assay) and lactate dehydrogenase (LDH) assay, respectively. The effects of nanoparticles on inflammatory responses are determined by secretion of inflammatory biomarkers, such as IL-8, IL-6, and tumor necrosis factor-alpha (TNF-α).[24] The inflammatory responses can also be evaluated by activation of platelets and macrophages.[23] Instillation of silica nanoparticles induced transient, but severe lung inflammation at an early stage and chronic granulomatous inflammation at the later stage in A/J mice. Cytokines and chemokines increased during the early stages, but decreased to basal level after 1 week (TNF-α) or 4 weeks (IL-1β, IL-6, IL-8, MCP-1 and MIP-2).[25] Our results showed that N-Epo-FePt prevented N-Epo-induced platelet activation, $CD68^{+}$-macrophage differentiation in blood, and intracellular ROS generation in MSCs (Fig. 3). The results from functional assays revealed that apoptotic cell death was increased and migration and MMP-9 activities were inhibited by N-Epo, but mot by N-Epo-FePt in MSCs (Figs. 6 and 7). These data indicated that inflammatory induction and toxicity were lower in FePt-decorated nano-epoxy nanoparticles than that in nano-epoxy nanoparticles.

Several factors have been reported to affect toxicity of nanoparticles, including association of cell surface to damage cell membrane or activate internal signaling pathways, dissolution of composites to release toxic ions, and generation of ROS to induce oxidative stress.[26] Treating human bronchoalveolar carcinoma cells with silica nanoparticles (15–46 nm) resulted in increasing ROS generation and LDH release in a dosage-dependent manner.[27] Mitochondrial damage-mediated ROS increase was also observed in 43 nm nonmodified amorphous silica nanoparticles-treated HepG2 human hepatocellular carcinoma cells for 3 and 24 hours exposure.[28] In our study, conjugation of FePt to nano-epoxy nanoparticles (N-Epo-FePt) reduced ROS production in MSCs (Fig. 3E), suggesting that modification of N-Epo by FePt leads to reducing toxicity at least in part due to decrease of intracellular ROS in MSCs.

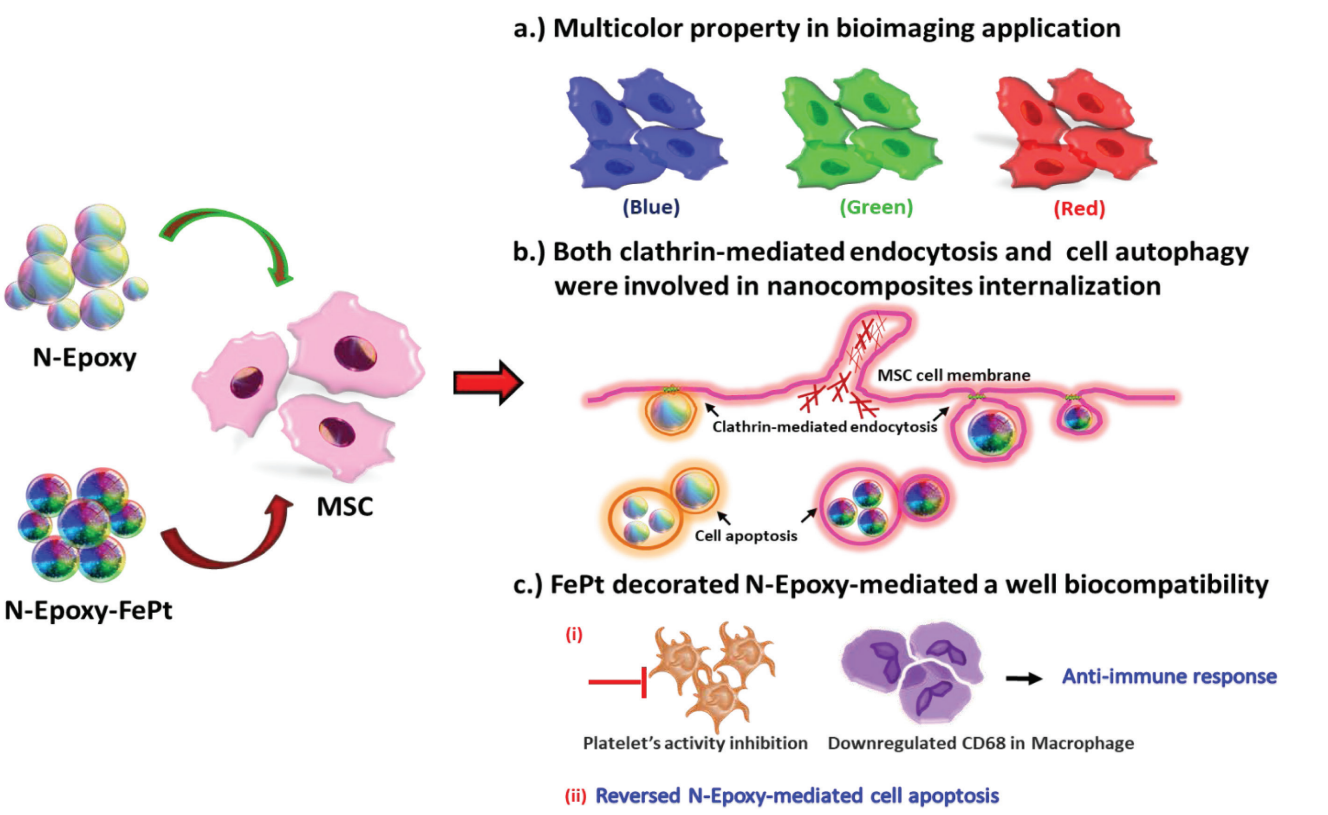

Fig. 8 Summary of the major findings. (A) Both N-Epo and N-Epo-FePt nanoparticles could be absorbed into MSCs. (B) The uptake of N-Epo and N-Epo-FePt into MSCs was mainly via clathrin-mediated endocytosis. (C) N-Epo-FePt was more biocompatible than N-Epo, as FePt-decorated N-Epo could prevent N-Epo-induced platelet activation, $CD68^{+}$-macrophage differentiation, intracellular ROS generation, and apoptosis of MSCs.

It has been reported that size, shape, and surface capping of gold nanoparticles (AuNPs) affect cytotoxicity in PC3 human prostate cancer cells. The cellular uptake by nanoparticle number was increased with decreased size of AuNPs. In terms of cytotoxicity, rod- and cube-shaped AuNPs were well tolerated, whereas spherical and prismatic AuNPs were toxic to PC3 cells.[29] Size-dependent cytotoxicity and genotoxicity were observed in silver nanoparticles (AgNPs) in HEI-OC1 cochlear cells. Comparing different sizes (5, 25, 50, and 110 nm) of AgNPs, the cytotoxicity and ROS production decreased with the increased size of nanoparticles. The higher level of DNA lesions measured by comet assay occurred after treatment with small-sized AgNPs (5 nm) in HEI-OC1 cells.[30] In the current study, the sizes in diameter of N-Epo-FePt and N-Epo were 177.38 ± 39.25 nm and 2.28 ± 1.01 nm, respectively (Fig. 2D, E). In addition to reduced ROS production, the lower cytotoxicity of N-Epo-FePt might be probably in part due to the larger size.

In conclusion, we developed the dual functional N-Epo-FePt nanoparticles by combining the fluorescent property of nano-epoxy and the magnetic characteristic of FePt. Both N-Epo and N-Epo-FePt nanoparticles could be absorbed into MSCs mainly through via clathrin-mediated endocytosis. FePt-decorated N-Epo could prevent N-Epo-induced platelet activation, CD68+-macrophage differentiation in blood, and reduce N-Epo-induced intracellular ROS generation, apoptosis, inhibition of cell migration, MMP-9 activity, and secretion of SDF-1α in MSCs. Thus, N-Epo-FePt was more biocompatible without altering biological performance than N-Epo in MSCs. These results suggest that N-Epo-FePt nanoparticle can be used for fluorescence labeling of MSCs and is potential to apply to bioimaging and cell tracking of MSCs *in vivo* by MRI or CT.

ACKNOWLEDGMENTS

This work was supported by grants from Ministry of Science and Technology, Taiwan (MOST-109-2314-B-039-046 and MOST 109-2320-B-039-015); Taichung Veterans General Hospital (TCVGH-1104902B and TCVGH-CTUST1107701) and China Medical University Hospital, Taiwan (DMR-110-133).

APPENDIX A. SUPPLEMENTARY DATA

Supplementary data related to this article can be found at http://links.lww.com/JCMA/A111.

REFERENCES

1. Gu H, Ma C, Gu J, Guo J, Yan X, Huang J, et al. An overview of multifunctional epoxy nanocomposites. *J Mater Chem C* 2016;**4**:5890–906.
2. Cerit A, Marti ME, Soydal U, Kocaman S, Ahmetli G. Effect of modification with various epoxide compounds on mechanical, thermal, and coating properties of epoxy resin. *Int J Polym Sci* 2016;**2016**:4968365.
3. Shi X, Nguyen TA, Suo Z, Liu Y, Avci R. Effect of nanoparticles on the anticorrosion and mechanical properties of epoxy coating. *Surf Coat Tech* 2009;**204**:237–45.
4. Hsiao K-T, Alms J, Advani SG. Use of epoxy/multiwalled carbon nanotubes as adhesives to join graphite fibre reinforced polymer composites. *Nanotechnology* 2003;**14**:791–3.
5. Tuncer E, Sauers I, James DR, Ellis AR, Paranthaman MP, Aytuğ T, et al. Electrical properties of epoxy resin based nano-composites. *Nanotechnology* 2006;**18**:02570.3
6. Tian W, Liu L, Meng F, Liu Y, Li Y, Wang F. The failure behavior of an epoxy glass flake coating/steel system under marine alternating hydrostatic pressure. *Corros Sci* 2014;**86**:81–92.

7. Toldy A, Szolnoki B, Marosi G. Flame retardancy of fibre-reinforced epoxy resin composites for aerospace applications. *Polym Degrad Stabil* 2011;**96**:371–6.
8. Hirabayashi Y, Hatta Y, Takeuchi J, Tsuboi I, Harada T, Ono K, et al. Novel three-dimensional long-term bone marrow culture system using polymer particles with grafted epoxy-polymer-chains supports the proliferation and differentiation of hematopoietic stem cells. *Exp Biol Med (Maywood)* 2011;**236**:1342–50.
9. Xue P, Bao J, Chuah YJ, Menon NV, Zhang Y, Kang Y. Protein covalently conjugated SU-8 surface for the enhancement of mesenchymal stem cell adhesion and proliferation. *Langmuir* 2014;**30**:3110–7.
10. Balmayor ER, Pashkuleva I, Frias AM, Azevedo HS, Reis RL. Synthesis and functionalization of superparamagnetic poly-ε-caprolactone microparticles for the selective isolation of subpopulations of human adipose-derived stem cells. *J R Soc Interface* 2011;**8**:896–908.
11. Lin P-Y, Hsieh S. One-step self-assembled epoxide-containing nanodots as an enzyme-immobilized platform for biosensing. *Sensor Actuat B-Chem* 2017;**240**:674–80.
12. Shi Y, Lin M, Jiang X, Liang S. Recent advances in fept nanoparticles for biomedicine. *J Nanomater* 2015;**2015**:467873.
13. Chou SW, Shau YH, Wu PC, Yang YS, Shieh DB, Chen CC. In vitro and in vivo studies of FePt nanoparticles for dual modal CT/MRI molecular imaging. *J Am Chem Soc* 2010;**132**:13270–8.
14. Liang S, Zhou Q, Wang M, Zhu Y, Wu Q, Yang X. Water-soluble L-cysteine-coated FePt nanoparticles as dual MRI/CT imaging contrast agent for glioma. *Int J Nanomedicine* 2015;**10**:2325–33.
15. Taylor RM, Huber DL, Monson TC, Ali AM, Bisoffi M, Sillerud LO. Multifunctional iron platinum stealth immunomicelles: targeted detection of human prostate cancer cells using both fluorescence and magnetic resonance imaging. *J Nanopart Res* 2011;**13**:4717–29.
16. Taylor RM, Sillerud LO. Paclitaxel-loaded iron platinum stealth immunomicelles are potent MRI imaging agents that prevent prostate cancer growth in a PSMA-dependent manner. *Int J Nanomedicine* 2012;**7**:4341–52.
17. Lin SZ. Advances in translational stem cell research and therapies. *Cell Transplant* 2011;**20**:1–3.
18. Saeedi P, Halabian R, Imani Fooladi AA. A revealing review of mesenchymal stem cells therapy, clinical perspectives and modification strategies. *Stem Cell Investig* 2019;**6**:34.
19. Tao R, Sun TJ, Han YQ, Xu G, Liu J, Han YF. Optimization of in vitro cell labeling methods for human umbilical cord-derived mesenchymal stem cells. *Eur Rev Med Pharmacol Sci* 2014;**18**:1127–34.
20. Dong NN, Pedroni M, Piccinelli F, Conti G, Sbarbati A, Ramírez-Hernández JE, et al. NIR-to-NIR two-photon excited CaF2:Tm3+,Yb3+ nanoparticles: multifunctional nanoprobes for highly penetrating fluorescence bio-imaging. *ACS Nano* 2011;**5**:8665–71.
21. Gizzatov A, Hernández-Rivera M, Keshishian V, Mackeyev Y, Law JJ, Guven A, et al. Surfactant-free Gd(3+)-ion-containing carbon nanotube MRI contrast agents for stem cell labeling. *Nanoscale* 2015;**7**:12085–91.
22. Lin CM, Kao WC, Yeh CA, Chen HJ, Lin SZ, Hsieh HH, et al. Hyaluronic acid-fabricated nanogold delivery of the inhibitor of apoptosis protein-2 siRNAs inhibits benzo[a]pyrene-induced oncogenic properties of lung cancer A549 cells. *Nanotechnology* 2015;**26**:105101.
23. Hung HS, Tang CM, Lin CH, Lin SZ, Chu MY, Sun WS, et al. Biocompatibility and favorable response of mesenchymal stem cells on fibronectin-gold nanocomposites. *PLoS One* 2013;**8**:e65738.
24. Bahadar H, Maqbool F, Niaz K, Abdollahi M. Toxicity of nanoparticles and an overview of current experimental models. *Iran Biomed J* 2016;**20**:1–11.
25. Cho WS, Choi M, Han BS, Cho M, Oh J, Park K, et al. Inflammatory mediators induced by intratracheal instillation of ultrafine amorphous silica particles. *Toxicol Lett* 2007;**175**:24–33.
26. Buchman JT, Hudson-Smith NV, Landy KM, Haynes CL. Understanding nanoparticle toxicity mechanisms to inform redesign strategies to reduce environmental impact. *Acc Chem Res* 2019;**52**:1632–42.
27. Lin W, Huang YW, Zhou XD, Ma Y. In vitro toxicity of silica nanoparticles in human lung cancer cells. *Toxicol Appl Pharmacol* 2006;**217**:252–9.
28. Sun L, Li Y, Liu X, Jin M, Zhang L, Du Z, et al. Cytotoxicity and mitochondrial damage caused by silica nanoparticles. *Toxicol in Vitro* 2011;**25**:1619–29.
29. Carnovale C, Bryant G, Shukla R, Bansal V. Identifying trends in gold nanoparticle toxicity and uptake: size, shape, capping ligand, and biological corona. *ACS Omega* 2019;**4**:242–56.
30. Perde-Schrepler M, Florea A, Brie I, Virag P, Fischer-Fodor E, Vâlcan A, et al. Size-dependent cytotoxicity and genotoxicity of silver nanoparticles in cochlear cells in vitro. *J Nanomater* 2019;**2019**:6090259.